Current Science
CS 5 (4), 3774-3793 (2025)
Received 14 May 2025 | **Revised 13 June** 2025 | **Accepted 15 July**. 2025 | **Online Available 1 August** 2025
https://doi.org/ 10.52845/CS/2025-5-4-37

Current Science

Current Science

OPEN ACCESS

ISSN(O)2795-8639

Original Article

Structural Response Analysis of Runner Blade Adjustment Mechanism of Kaplan Turbine by Modal Decomposition and Function-Driven

Zhe Zhang[1], Houyu Zhang[2], Yingbo Guan[2], Mingkun Fang[3], Di Zhu[1,*], Ran Tao[3]

[1]College of Engineering, China Agricultural University, Beijing, China

[2]State Grid Fujian Electric Power Research Institute Fuzhou, Fujian, China

[3]College of Water Resources and Civil Engineering, China Agricultural University, Beijing, China

[*]Corresponding Author: Di Zhu

Abstract:
This study focuses on runner blades of hydraulic turbines, aiming to achieve accurate prediction of blade torque and structural stress analysis under eight operating conditions through fluid-structure interaction analysis. A combined method of Variational Mode Decomposition (VMD) and Long Short-Term Memory (LSTM) network is adopted to process blade torque signals: VMD decomposes complex torque time-series signals into intrinsic mode functions with different frequency characteristics, while LSTM network, leveraging its advantage in capturing long-term dependencies in sequence data, reconstructs precise torque variation patterns, with the root mean square error (RMSE) ranging from 0.02% to 0.51% across all operating conditions, fully verifying its effectiveness. Stress analysis shows that there are three key high-stress areas in Kaplan turbines, namely the corner of the tumbler arm, the middle part of the side surface of the connecting plane, and the diameter-changing section of the thin shaft on the ear lug, among which the diameter-changing section of the thin shaft on the ear lug has the highest stress level and should be the key target for structural optimization. Correlation analysis indicates that when the runner blade angle is 0° and -5°, stress fluctuations are the most drastic, while an increase in the angle (e.g., exceeding -5°) can significantly improve operational stability, and combining stress analysis with the full characteristic diagram of the hydraulic turbine can effectively delineate safe and stable operating regions. The results demonstrate that the VMD-LSTM framework can efficiently complete torque prediction with limited computational resources, and the stress analysis results provide targeted guidance for structural reinforcement, offering important references for the design optimization, durability improvement, and safe operation of hydraulic turbines under different hydrological conditions.

Keywords: Hydraulic Turbine; Runner Blade; Fluid-Solid Interaction; Modal Decomposition; Neural Network

Introduction

Hydropower is a relatively early - emerging clean energy utilization method, and the related technologies are quite mature, becoming an indispensable part of electricity production. The core of hydropower generation lies in the water turbine, which efficiently and stably converts the mechanical energy of water into electrical energy [1]. Therefore, the rational design of the water turbine is extremely important. Kaplan turbines are suitable for hydropower generation scenarios with small upstream-downstream water level differences (water heads) but large flow rates [2]. Due to the small water head difference, even a slight change in the water head is extremely obvious [3, 4]. For example, the applicable water head range of most Kaplan turbines is 10-50 m, and a 2 m change in the water head may cause a 4%-20% deviation in working conditions. In order

to adapt to the operational instability caused by this deviation in working conditions, the blades of many large and medium sized Kaplan turbines are designed to have an adjustable opening. The hydraulic mechanism drives components such as the operating frame, lug, connecting rod, and rotating arm, converting the up and down movement of the piston rod into the rotation of the blades [5]. This design is extremely ingenious, widening the efficient operation range of the Kaplan turbine and enhancing its adaptability to working conditions [6].

The design of the blade adjustment mechanism is extremely important for Kaplan turbines, which is reflected in two aspects. Firstly, the main function of the blade adjustment mechanism is to convert the movement of the operating frame into the rotation of the blades. Its movement law needs to be as simple as possible, and the adjustment needs to be as direct and easy to control as possible. Secondly, the strength of the blade adjustment mechanism must meet the requirements to avoid fatigue damage or plastic deformation in a short period. Generally speaking, the latter is relatively simple to achieve, but this has instead become a major hidden danger. With the increasing demand for peak shaving in the power system, the frequent start-stop and variable-condition operation of water turbines have become the norm. Especially with the introduction of Automatic Generation Control (AGC) technology [7, 8], the blade adjustment mechanism continuously adjusts itself with changes in working conditions, causing a series of components from the blades to the operating frame to continuously bear the coupled loads of multiple physical fields such as transient water flow impact and mechanical vibration [9]. This may make each component of the originally designed adjustment mechanism unable to adapt to the new requirements. According to statistics, the proportion of unplanned shutdown accidents of hydropower units worldwide caused by dynamic instability or fatigue fracture of the adjustment mechanism is close to 30%, resulting in huge economic losses [10]. Therefore, accurately predicting the dynamic response characteristics of the blade adjustment mechanism and revealing the spatial - temporal correlation mechanism between it and external loads has become a key scientific issue for ensuring the safe operation of water turbines.

In fact, many researchers have conducted in-depth studies on the response characteristics of structural components under variable fluid loads. The dynamic response prediction of bridges under wind loads is a typical case. In 1961, Davenport deeply studied the statistical characteristics of random wind loads, established the probability distribution models of wind speed and wind pressure by using probability theory and mathematical statistics, and revealed the random variation law and extreme value distribution characteristics of wind loads, laying a solid theoretical foundation for subsequent research in the field of wind engineering and the development of random wind load simulation technology [11, 12, 13].

The structural response of aero-engine cascades under thermal fluid action is another typical scenario. Zhang et al. [14] studied the structural response of aero-engine turbine cascades under high temperature thermal fluids, analyzed the influence of thermal fluids on the cascade structure by combining experiments and numerical simulations, and revealed the deformation law and stress distribution characteristics of the cascade under thermal fluids, providing a scientific basis for the thermal protection and structural design optimization of aero - engine cascades. Gong et al. [15] experimentally studied the influence of slotted wake plates on the flow field of transonic turbine planar cascades, measured the flow field characteristics inside the cascade under different working conditions, analyzed the flow structure and pressure distribution of the cascade under thermal fluid action, and found that slotted wake plates can improve the internal flow of the cascade and reduce aerodynamic losses, providing technical references for the performance improvement of turbine cascades. Lin et al. [16] explored the hypersonic wind tunnel pressure sensitive paint (PSP) test technology, measured the surface pressure distribution of aero-engine cascades under thermal fluids using PSP technology, and analyzed the pressure variation laws on the cascade surface under different thermal fluid conditions, providing experimental data support for the aero thermodynamic performance evaluation and structural response analysis of cascades.

The fluid structure interaction (FSI) behavior of

wind turbine towers and blades during operation is also a current research hotspot. Li et al. [17] studied the dynamic response characteristics of wind turbine airflow FSI under typhoon wind speeds, analyzed the loads and response characteristics of wind turbines under different wind speeds through numerical simulations using an improved FSI method, revealed the influence law of wind speed increase on the fluctuation amplitude of blade thrust and torque loads, and found structural buckling phenomena on the suction surface of blades, providing a scientific basis for the structural reliability research of wind turbine blades in typhoon environments. Zhang et al. [18] analyzed the wind-earthquake coupling response of wind power tower structures considering blade rotation effects, generated wind speed sequences using the harmonic superposition method, calculated impeller loads considering blade rotation effects based on the blade element momentum (BEM) theory, calculated wind loads on the tower surface combined with a wake model, established a finite element model considering blade eccentricity and nacelle concentrated mass, analyzed the response of wind power towers under wind - earthquake coupling, and revealed the influence of blade rotation effects and wake on wind load calculation, providing technical support for the seismic design of wind power towers. Gong et al. [19] discussed the FSI analysis of large-scale wind turbines under yaw conditions, studied the coupled dynamic behavior of wind turbine blades and towers under yaw conditions using an improved BEM and finite element method, analyzed the stress distribution and vibration characteristics of blades and towers, and provided references for the structural design and safety assessment of large-scale wind turbines under complex wind direction conditions.

In the field of water turbines, there are many studies on the structural response of runner blades, as well as research on guide vanes, main shafts, crowns, bolts, etc., which have achieved rich conclusions. Wang et al. [20] used a hybrid method of improved discrete vortex and geometrically exact beam theory to analyze the structural dynamic response of a three bladed vertical axis water turbine. Compared with the traditional finite element method, this method has the advantages of fast solution, simple modeling, and high calculation accuracy. In the modal analysis, the first five natural frequencies of the turbine blades and the whole machine under different blade heights were calculated, and the influence of the turbine radius and blade height on the natural frequencies was analyzed. The results showed that with the increase of size, the natural frequencies of the blades and the whole machine decreased significantly, and the whole machine natural frequency was more affected by the radius size. In the transient analysis, considering the centrifugal load and the hydrodynamic load of the blades, the maximum deformation curve of the blades during one rotation under working conditions was obtained; the blade strength problem under different *H/R* (blade height-to-radius ratio) was analyzed. The results showed that when *H/R* is greater than 3.0, the blade strength will fail.

Gui et al.[21] analyzed the dynamic stress of the runner during the start-up process of a pump - turbine, and carried out a study on the fluid - structure coupling dynamic characteristics of the pump-turbine during the transient process using numerical simulation technology. First, a method for identifying structural response and modal analysis under cavitation conditions based on acoustic - structure coupling was proposed, and its applicability and accuracy in structural modal calculation under cavitation conditions were verified by comparing with experimental results and traditional modal analysis methods. Based on this method, the influence of cavitation void fraction on natural frequency, mode shape, and response was discussed, and the mechanism of modal separation was expounded. Second, taking the prototype unit of the pump - turbine as the research object, the flow field characteristics during the start - up process of the pumping condition and the generating condition were simulated. Considering the unsteady flow of kilometer-scale pipelines and millimeter-scale runner clearances, the reliability of the calculation method was verified by comparing with the measured results, and a calculation method for the axial water thrust of the runner in the multi-scale full flow field during the transient process of the pump - turbine was proposed. Finally, based on the flow field characteristics, the structural characteristics of the upper frame, shaft system, and runner of the pump-turbine under the influence of circumferentially asymmetric hydraulic excitation during the transient process

were calculated. It was found that the circumferentially asymmetric water thrust would lead to the circumferentially asymmetric distribution of the runner's own displacement, and the action on the upper frame through the shaft system was mainly reflected in the resultant axial water thrust, which was not affected by the distribution of water thrust, in line with Saint-Venant's principle. During the start - up process of the pump and turbine conditions, stress concentration occurred at the connection between the support rib plate and the thrust bearing seat of the upper frame. In the early stage of the pump condition start-up process, the stress concentration of the runner was located at the connection between the crown and the blade inlet, and later at the connection between the crown and the blade outlet; during the start-up process of the turbine condition, before the guide vanes are opened to the no-load opening, the stress concentration of the runner is located at the connection between the band and the runner inlet, and during the load-increasing stage, it is located at the connection between the crown and the runner inlet, and finally moves to the connection between the band and the runner outlet.

Liu et al. [22] obtained the modal parameters of the guide vanes through modal testing and analysis, including natural frequency, mode shape, and damping coefficient, which can provide a basis for the vibration characteristic analysis, vibration fault diagnosis and prediction, and structural dynamic characteristic optimization design of the hydropower unit system. For the guide vanes of the water turbine, the frequency response function was obtained through modal testing and analysis using the MIMO method, and five order modal parameters were obtained by fitting, including natural frequency, mode shape, and damping coefficient, providing a reference for the fault diagnosis of the water turbine and the dynamic characteristic research of the guide vanes.

In summary, studies on structural response based on fluid-structure interaction (FSI) analysis are feasible, but they consume heavy computational resources. Especially for the dynamic response of Kaplan turbine blade adjustment mechanisms, due to the complexity of mathematical models, related research remains scarce. If simplified methods can be used to solve problems in water turbines, it will provide better solutions for relevant engineering issues. The key to the above analysis lies in the effective analysis of force and moment load laws. If effective analysis is not possible, it must be replaced by complex and time-consuming iterative calculations. The variation of fluid loads is a common physical phenomenon, which contains both regular and irregular components [23]. The key to analyzing this complex signal lies in the extraction of regular patterns and the identification of noise components. Modal decomposition provides a solution to this problem. In recent years, the proposal and improvement of methods such as Empirical Mode Decomposition (EMD) and Variational Mode Decomposition (VMD) have undoubtedly been successful [24, 25]. Based on Hilbert transform and other methods, physical quantities such as forces and moments are decomposed by frequency and attributed to multiple modes guided by typical central frequencies. Modal decomposition is particularly suitable for the load analysis of Kaplan turbine blade adjustment mechanisms. Each decomposed sub-mode has its own frequency characteristics [26], which can be modeled and constructed using trigonometric functions. Finally, the non-decomposable noise modes can be effectively excluded and redundant information removed, an operation that is extremely effective for fatigue damage characteristic analysis, as periodic factors are sufficiently emphasized.

Aiming at the above bottlenecks, this paper proposes a dynamic response prediction framework of "Variational Mode Decomposition (VMD)-Function Reconstruction-Transient Simulation", taking the blade adjustment mechanism of a large axial flow turbine as the research object, and carrying out a systematic study based on the measured moment data under 10 typical working conditions. First, the VMD algorithm is used to adaptively decompose the non-stationary torque time-series signals and construct their mathematical expressions. Then, dominant modes are screened by energy proportion, non-linearly fitted for sub-mode components, explicit equations of moment-time relationships are established, and equivalent load time-series are generated. Furthermore, the reconstructed signals are used as boundary conditions for structural finite element analysis. Finally, by comparing the stress peaks and

displacement fluctuation laws under different step sizes, the fatigue risk thresholds of key components such as the lug and connecting rod of Kaplan turbine are quantified, and a "working condition-response" prediction model based on LSTM network is constructed. This paper provides theoretical support for the optimal design, intelligent operation and maintenance, and life prediction of turbine blade adjustment mechanisms, and is of great significance for improving the operation safety and economy of hydropower stations.

2 Research Objective

2.1 Basic Parameter of Kaplan Turbine

In this case, the research objective is a Kaplan turbine as shown in Fig. 1. The basic parameter of this turbine is listed in Table 1. As shown, the rated power is about 235.0 MW and the rated flow rate is 83.3 m^3/s. The rated water head is about 47.0 m and the maximum water head is about 57.8 m which are relatively mid-high for Kaplan turbine usage. The runner diameter is about 8.0 m and has 6 blade in total. As indicated by the *X-Y-Z* Global Cartesian coordinate, the rotation of runner is around the *Z* axis. The rotation speed is 107.1 r/min with the direction shown in in Fig. 1. The other important parameters are all listed in Table 1. Extracted from the general domain of runner body, the runner blade adjustment mechanism is the main focused objective. It includes the ear lug, connecting plate, tumbler, and runner blade.

Table 1 Basic parameter of Kaplan turbine

Parameter	Symbol	Unit	Value
Rated Water Head	H_r	m	47.0
Maximum Water Head	H_{max}	m	57.8
Minimum Water Head	H_{min}	m	31.0
Rated Flow Rate	Q_r	m^3/s	83.3
Rated Rotation Speed	n_r	r/min	107.1
Rated Power	P_r	MW	235.0
Runner Diameter	D_1	m	8.0
Runner Blade Number	b_{rn}	-	6

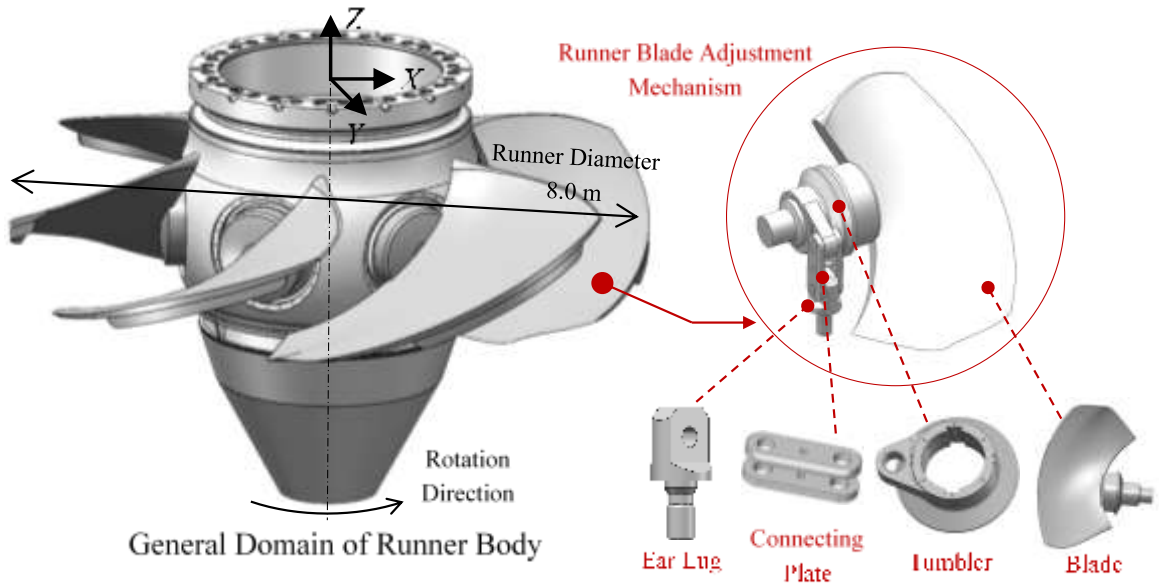

Figure 1 The research objective of Kaplan turbine

2.2 Kinematics Relationship of Blade Adjustment

Figure 2 illustrates the blade adjustment mechanism of a Kaplan turbine. This mechanism is composed of ear lug, connecting plate, tumbler, blade, and runner hub shown in a blurred manner. The servomotor operating force F_S acts vertically on the lug. Driven by F_S, the connecting plate and the tumbler initiate motion, which enables the adjustment of the blade angle. In the meantime,

the blades are subjected to water thrust F_Z, and the tumbler bears the blade hydraulic moment M_S is a rotational moment generated by the blades' interaction with water flow.

During operation, the blades are subjected to water thrust F_Z generated by hydrodynamic interaction, which, combined with the structural characteristics of the mechanism, produces a blade hydraulic moment M_S which is a rotational moment acting on the tumbler. These three key parameters (F_S, F_Z, and M_S) facilitate precise control over blade angles through the transmission of forces and conversion of motion, enabling the adjustment mechanism to maintain optimal hydrodynamic performance and mechanical equilibrium.

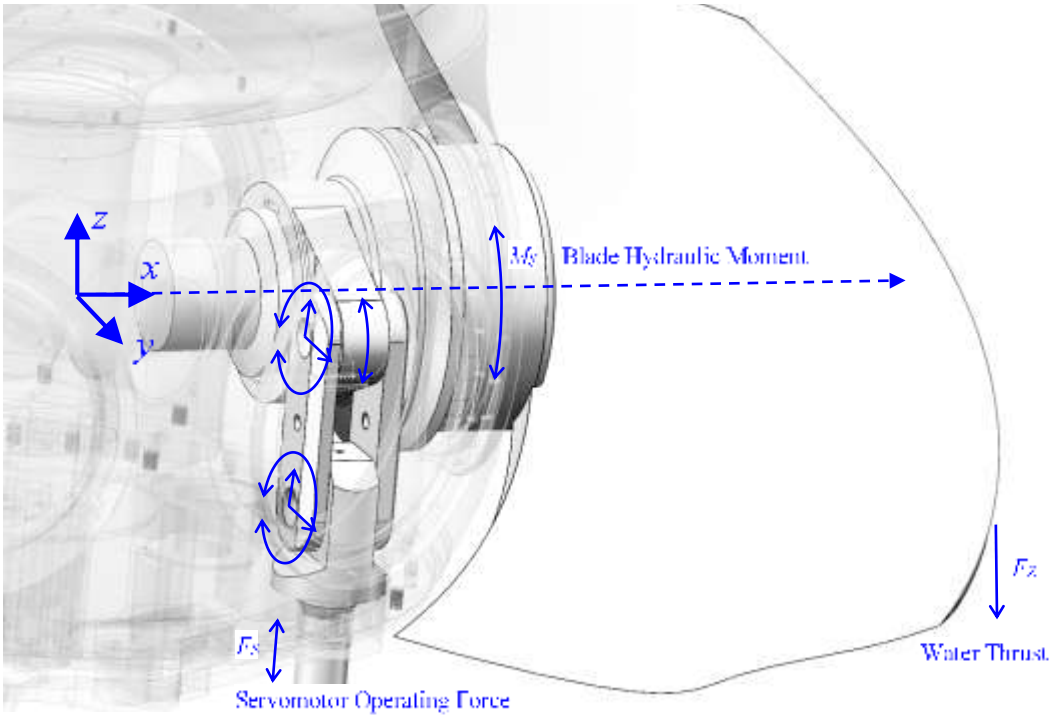

Figure 2 Blade adjustment mechanism

3 Methodology of Investigation

3.1 Fluid-Solid Interaction

The dynamic methodology for examining of the structural responses requires an analysis of the temporal progression and frequency features of the external forces. The transient dynamic equilibrium equations for linear structures is written as follows:

$$[M]\{\ddot{u}\}+[C]\{\dot{u}\}+[K]\{u\}=\{F^a\} \quad (1)$$

where [M], [C], and[K] denote the structural mass, damping, and stiffness matrices, $\{u\}$, $\{\dot{u}\}$, and $\{\ddot{u}\}$ represent the nodal displacement, velocity, and acceleration vectors, respectively. The external load vector $\{F^a\}$ encompasses various forces acting on the node, such as pressure, gravitational, and centrifugal forces. Eq. (1) is solved using the Newmark algorithm as below:

Within the time interval Δt, the finite difference expansions of $\{\dot{u}_{n+1}\}$, $\{\dot{u}_{n+1}\}$ are carried out and approximated as:

$$\{\dot{u}_{n+1}\}=\{\dot{u}_n\}+[(1-\delta)\{\ddot{u}_n\}+\delta\{\ddot{u}_{n+1}\}]\Delta t \quad (2)$$

$$\{u_{n+1}\}=\{u_n\}+\{\dot{u}_n\}\Delta t+\left[\left(\frac{1}{2}-\alpha\right)\{\ddot{u}_n\}+\alpha\{\ddot{u}_{n+1}\}\right]\Delta t^2 \quad (3)$$

The subscript n denotes the present time instant, while n+1 signifies the subsequent time instant,

and α and δ are constants. The two equations (2) and (3) are combined as Eq. (4) and (5) and the transient power balance equations for the moment n+1 are Eq. (6):

$$\{\dot{u}_{n+1}\} = \{\dot{u}_n\} + a_6\{\ddot{u}_n\} + a_7\{\ddot{u}_{n+1}\} \quad (4)$$

$$\{\ddot{u}_{n+1}\} = a_0(\{u_{n+1}\} - \{u_n\}) - a_2\{\dot{u}_n\} - a_3\{\ddot{u}_n\} \quad (5)$$

$$[M]\{\ddot{u}_{n+1}\} + [C]\{\dot{u}_{n+1}\} + [K]\{u_{n+1}\} = \{F^a\} \quad (6)$$

Substituting them gives:

$$(a_0[M] + a_1[C] + [K])\{u_{n+1}\} = \{F^a\} + [M](a_0\{u_n\} + a_2\{\dot{u}_n\} + a_3\{\ddot{u}_n\}) + [C](a_1\{u_n\} + a_4\{\dot{u}_n\} + a_5\{\ddot{u}_n\}) \quad (7)$$

where $a_0 = \frac{1}{\alpha\Delta t^2}$, $a_1 = \frac{\delta}{\alpha\Delta t}$, $a_2 = \frac{1}{\alpha\Delta t}$, $a_3 = \frac{1}{2\alpha} - 1$, $a_4 = \frac{\delta}{\alpha} - 1$, $a_5 = \frac{\Delta t}{2}\left(\frac{\delta}{\alpha} - 2\right)$, $a_6 = \Delta t(1-\delta)$, $a_7 = \delta\Delta t$, $\alpha \geq \frac{1}{4}\left(\frac{1}{2} + \delta\right)^2$.

When the parameters α and δ are such that $\delta \geq \frac{1}{2}$ and $\frac{1}{2} + \delta + \alpha > 0$, Eq. (7) stably converges. Initial displacement condition is:

$$\{u_0\} = \begin{cases} \{0\} & \text{No available previous result or initial condition.} \\ \{u_s'\} & \text{Have initial conditions, No available previous result.} \\ \{u_s\} & \text{Have initial conditions and available static previous result.} \end{cases} \quad (8)$$

Within the context, $\{\ddot{u}_0\} = \{0\}$ and$\{\dot{u}_0\}$ signifies the initial velocity, while $\{\bar{u}_s'\}$ denotes the velocity defined by the initial conditions. $\{u_s\}$ represents the displacement from the preceding static calculation stage, and $\{u_s–1\}$ corresponds to the displacement at the time instant prior to $\{u_s\}$. For the first computation of $\{u_s\}$, $\{u_s–1\}$is 0; $\Delta t = t_s – t_s–1$. Initial acceleration $\{\ddot{u}_0\} = \{0\}$. Then, it is able to calculate the displacement $\{u\}$. From this displacement, the nodal stress σ for each time instant is derived, followed by the computation of the equivalent stress σ_e.

3.2 Variational Mode Decomposition

To efficiently extract characteristic features from complex signals, this research employs the Variational Mode Decomposition (VMD) approach. It was proposed as an adaptive decomposition methodology specifically designed for non-stationary signals. This methodology utilizes an iterative optimization scheme to identify the optimal variational model, hypothesizing that the target wind turbine active power signal consists of multiple Intrinsic Mode Function (IMF) components. Each component displays amplitude-modulated and frequency-modulated (AM-FM) characteristics, accompanied by mathematically constrained spectral properties.

Initially, the Hilbert transform is applied to each modal function, thereby enabling the acquisition of analytical values for distinct modal functions.

$$\left(\delta(t) + \frac{j}{\pi t}\right) * u_k(t) \quad (9)$$

Then, the center frequency of the aforementioned equation is evaluated and combined with a complex exponential function, thereby shifting the spectral distribution of each modal function to their corresponding frequency basebands, resulting in:

$$\left[\left(\delta(t)+\frac{j}{\pi t}\right)*u_k(t)\right]e^{-j\omega_k t} \quad (10)$$

Through the application of the Hilbert transform in the frequency domain for processing the acquired wind turbine active power data, the constrained variational optimization problem is derived as follows:

$$\min_{\{u_k\},\{\omega_k\}}\left\{\sum_k \partial_t\left[\left(\delta(t)+\frac{j}{\pi t}\right)*u_k(t)\right]e^{-j\omega_k t}\right\}_2^2 \quad (11)$$

Where u_k, ω_k are the modal functions and central frequencies respectively (k∈1, 2, ..., K); K is the number of modes obtained from decomposition; ∂_t is the gradient operation; $\delta(t)$ is the unit impulse function; t is time; j is the imaginary unit; e is the base of the natural logarithm.

Through the introduction of a quadratic penalty function α and a Lagrange multiplier λ, the aforementioned constrained optimization problem is converted into an unconstrained optimization problem as:

$$\begin{aligned}L(\{u_k\},\{\omega_k\},\lambda) &= \alpha\sum_k \partial_t\left[\left(\delta(t)+\frac{j}{\pi t}\right)*u_k(t)\right]e^{-j\omega_k t}\Big\|_2^2 \\ &+\Big\| f(t)-\sum_k u_k(t)\Big\|_2^2 + \langle \lambda(t), f(t)-\sum_k u_k(t)\rangle\end{aligned} \quad (12)$$

The minimization problem is transformed into a saddle-point problem, the initialization formulas for $\{u_k\}$, $\{\omega_k\}$, and λ of each sub-signal introduced by the alternating direction multiplier method are:

$$u_k^{n+1}(\omega)=\frac{\hat{f}(\omega)-\sum_{i\neq k}\hat{u}_i^{n+1}(\omega)+\frac{\hat{\lambda}^n(\omega)}{2}}{1+2\alpha\left(\omega-\omega_k^n\right)^2} \quad (13)$$

$$u_k^{n+1}(\omega)=\frac{\int_0^\infty \omega\left|\hat{u}_k^{n+1}(\omega)\right|^2 d\omega}{\int_0^\infty\left|\hat{u}_k^{n+1}(\omega)\right|^2 d\omega} \quad (14)$$

$$\hat{\lambda}^{n+1}(\omega)=\hat{\lambda}^n(\omega)+\left(\hat{f}(\omega)-\sum_k\hat{u}_k^{n+1}(\omega)\right) \quad (15)$$

where τ is the update factor for the Lagrange multiplier, and n represents the iteration number n ={1, ..., N}. The iteration stops when:

$$\sum_k\left\|\hat{u}_k^{n+1}-\hat{u}_k^n\right\|_2^2 / \left\|\hat{u}_k^n\right\|_2^2 < \varepsilon \quad (16)$$

3.3 Fitting and Reconstruction

The fundamental principle of fitting functions is primarily grounded in the least squares approach and the Levenberg-Marquardt (L-M) iterative algorithm. The least squares method represents a mathematical optimization approach employed to determine the optimal fitting curve, which minimizes the aggregate of squared discrepancies between the curve and data points. The L-M iterative algorithm, a nonlinear optimization

technique, integrates the merits of gradient descent and the Gauss-Newton method, rendering it efficient for identifying optimal parameter values.

Function fitting principles primarily rely on the least squares approach and the Levenberg-Marquardt (L-M) iterative algorithm. The least squares method, a mathematical optimization strategy, aims to identify the optimal curve by minimizing the cumulative squared deviations between the curve and observed data points. Meanwhile, the L-M iterative algorithm—a hybrid nonlinear optimization technique-integrates the strengths of gradient descent and the Gauss-Newton method, enabling efficient convergence to optimal parameter configurations.

The least squares approach represents a mathematical optimization strategy that determines the optimal fitting curve for a collection of data points by minimizing the aggregate of squared residuals. Consider a dataset consisting of points (x_i, y_i), i=1,2, …, n. Our goal is to model these points using a function $y=f(x)$. The core objective of the least squares method is to minimize the sum of squared residuals S, which is formulated as:

$$S=\sum_{i=1}^{n}(y_i - f(x_i)) \qquad (17)$$

To determine the parameters that optimize S, partial derivatives of S are computed with respect to each parameter and subsequently set to zero. For example, in the context of a linear regression model $y=ax+b$, the derivatives are calculated for parameters a and b as follows:

$$\frac{\partial S}{\partial a} = -2\sum_{i=1}^{n}(y_i - ax_i - b)\,x_i = 0 \qquad (18)$$

$$\frac{\partial S}{\partial b} = -2\sum_{i=1}^{n}(y_i - ax_i - b) = 0 \qquad (19)$$

Solving this system of equations derives the optimal parameters a and b.

The L-M algorithm serves as an iterative approach for addressing non-linear least squares problems, integrating the merits of gradient descent and the Gauss-Newton method. The fundamental concept involves tuning parameters β in each iteration to minimize the objective function $S(\beta)$, following the update formula:

$$\beta_{k+1} = \beta_k + \Delta\beta \qquad (20)$$

$$(J^T J + \lambda I)\Delta\beta = J^T r \qquad (21)$$

where J represents the Jacobian matrix, r signifies the residual vector, and λ acts as a damping coefficient that balances the influences of gradient descent and the Gauss-Newton approach. The initial parameter values β_0 must be appropriately specified, with iterations proceeding until the residuals satisfy the convergence conditions or the maximum iteration is attained.

3.4 Long-Short Term Memory

Developed to tackle the gradient vanishing and exploding issues in RNN architectures, the Long Short-Term Memory (LSTM) model demonstrates significantly better performance in sequence data prediction and classification tasks. Unlike traditional RNNs, which employ Back Propagation Through Time (BPTT) for training but retain minimal information from initial sequence segments thereby impacting weight updates LSTM replaces each RNN hidden unit with a memory-encoded cell. Each cell comprises three key components: input, forget, and output gates. While input and output gates control

information flow, the forget gate governs internal state information. The workflow of RNN and LSTM are shown in Fig. 3.

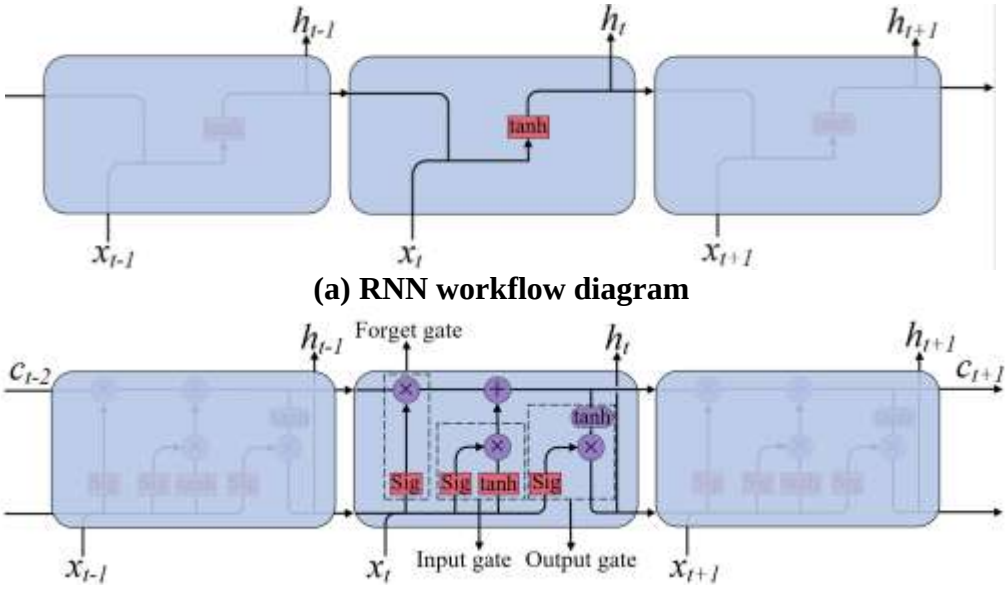

(a) RNN workflow diagram

(b) LSTM workflow diagram

Figure 3 Workflow diagrams of RNN and LSTM

The initial step of LSTM operation involves the utilization of a forget gate to selectively discard certain data.

$$f_t = \sigma\left(W_f x_t + U_f h_{t-1} + b_f\right) \tag{22}$$

The input gate assesses the extent to which the current input state facilitates information updates at the current time step. By integrating the switching values of the input gate and forget gate, modifications are made to the information retained in the memory cell.

$$i_t = \sigma\left(W_i x_t + U_i h_{t-1} + b_i\right) \tag{23}$$

$$\tilde{C}_t = \tanh\left(W_c x_t + U_c h_{t-1} + b_c\right) \tag{24}$$

The refreshed cell state is determined by integrating the historical states of the forget gate and input gate:

$$C_t = f_t * C_{t-1} + i_t * \tilde{C}_t \tag{25}$$

The final output gate determines the information to be released at the current time step. This information first undergoes a linear transformation and is then fed into a sigmoid activation function, thereby determining the switching value of the output gate:

$$o_t = \sigma\left(W_o\left[h_{t-1}, x_t\right] + b_o\right) \tag{26}$$

$$h_t = o_t * \tanh\left(C_t\right) \tag{27}$$

The aforementioned equations incorporate the weight matrix W_f, the weight matrix associated with the previous time step U_f, and the bias vector b_f. These parameters are explicitly employed to compute the forget gate's switching value at the current time step. Conversely, W_i, U_i, and bi

denote the weight matrix and bias vector of the input gate, which are utilized to determine the input gate's switching value at the current time step. Meanwhile, W_c, U_c, and $\underline{b_c}$ are tasked with calculating the candidate memory for the current time step. W_o, U_o, and b_o correspond to the weight matrix and bias vector of the output gate, respectively, used to derive the output gate's switching value at the current time step. The variables f_t, i_t, and o_t symbolize the computed outcomes of the forget gate, input gate, and output gate at time step t, respectively. The sigmoid activation function, confined between 0-1, is mathematically expressed as:

$$\sigma(x) = \frac{1}{1+e^{-1}} \tag{28}$$

4 Results and Analysis

4.1 Acquisition of CFD Torque Loading

This chapter presents the analysis of torque data obtained from Computational Fluid Dynamics (CFD) simulations. It is based on the general map of performance characteristics shown in Fig. 4 where b is the runner blade angle value whose unit is degrees. Around the high-efficiency region, 8 operation points named A~I are chosen as typical points for analysis. The CFD simulations were conducted for 720 time steps with a step size of 0.00156 seconds (total duration: 1.1232 seconds), generating high-resolution torque data for each operating condition. The torque characteristics are crucial for understanding the dynamic behavior of the turbine under various operating conditions. The data is visualized to generate a 2D temporal torque plots as shown in Fig. 5. It reflects a complex yet orderly state of fluctuation, which includes large-period fluctuations and high-frequency rapid changes. To better clarify the structural response characteristics, it is necessary to deeply analyze the torque changes applied to the blade structural components, and modal decomposition may be a good approach.

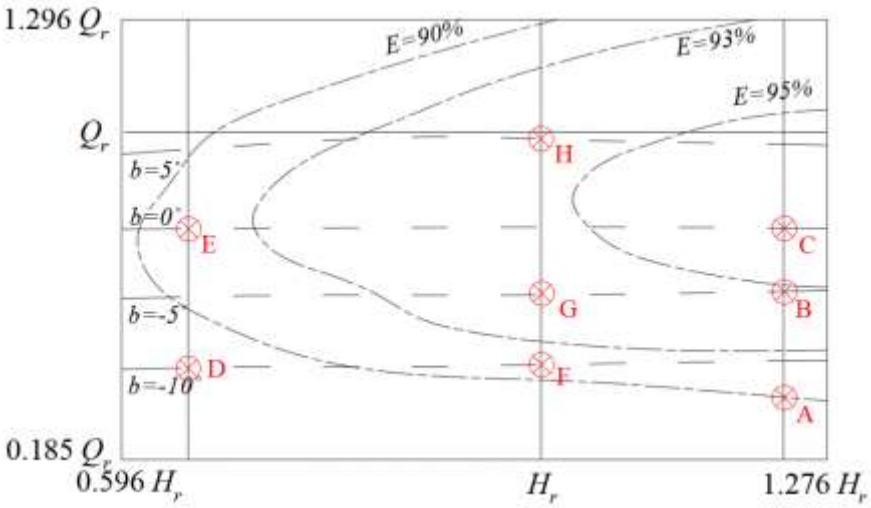

Figure 5 The general map of performance characteristics

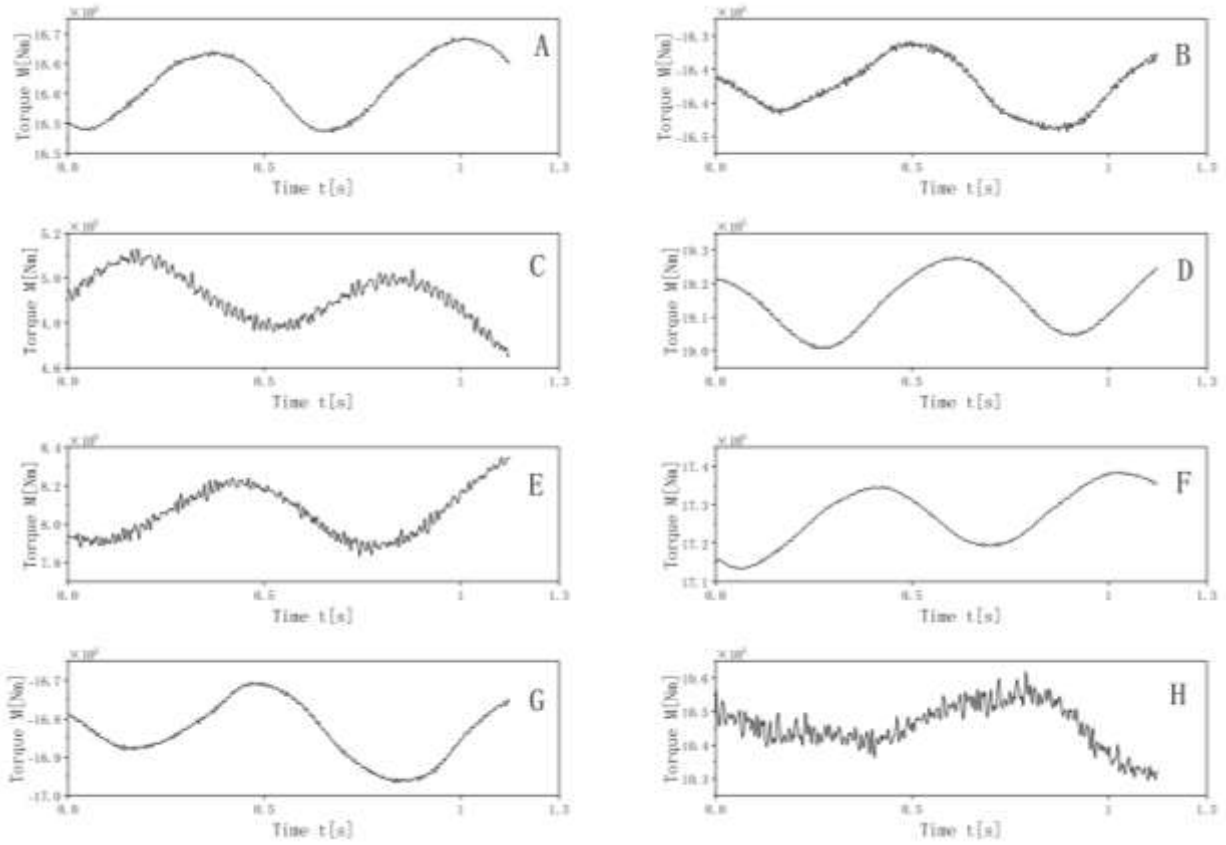

Figure 6 Temporal variation of blade torque

4.2 Mode Decomposition of Torque Data

Variational mode decomposition (VMD) is performed on the data to obtain different modes. Then, fitting is carried out for different modes. The fitted data will follow the equation as:

$$T_b = \sum_{i=1}^{n} [A_i \times sin(\omega_i \times t + \varphi_i)] + D \quad (29)$$

where A_i is the sinusoidal term coefficient, ω_i is the rotational angular velocity, φ_i is the phase angle and D is the combination constant. For each operation point, the value of coefficients are listed in Table 2.

Table 2 Value of coefficients

Condition	Sinusoidal Term Coefficient A_i	Rotational Angular Velocity ω_i	Phase Angle φ_i	Combination Constant D
A	-7.5586×10^{3}	9.7945×10^{0}	1.1009×10^{0}	1.6611×10^{6}
A	-1.9006×10^{3}	9.9227×10^{0}	-2.2021×10^{0}	
A	9.5146×10^{1}	2.6896×10^{2}	4.9705×10^{0}	
A	5.6842×10^{1}	2.6522×10^{2}	-14.8551×10^{0}	
B	5.0026×10^{3}	9.3580×10^{0}	3.1962×10^{0}	-1.6365×10^{6}
B	6.9452×10^{1}	2.0123×10^{2}	-5.8133×10^{0}	
B	9.4621×10^{1}	1.9782×10^{2}	2.1335×10^{0}	
C	1.4972×10^{4}	8.6026×10^{0}	4.1581×10^{-1}	4.8791×10^{5}
C	9.2000×10^{3}	4.3013×10^{0}	2.4040×10^{-2}	
C	2.0000×10^{3}	3.2577×10^{2}	1.8035×10^{1}	

D	1.0638×10^{4}	9.6923×10^{0}	2.2208×10^{0}	1.9167×10^{6}
D	1.9167×10^{6}	9.7884×10^{0}	2.4019×10^{1}	
D	1.2150×10^{2}	1.8762×10^{2}	-1.5886×10^{0}	
D	1.5650×10^{2}	1.9522×10^{2}	-3.9539×10^{0}	
E	-1.7359×10^{4}	9.0997×10^{0}	8.4051×10^{-1}	8.0654×10^{5}
E	2.0000×10^{3}	4.9522×10^{2}	6.4161×10^{1}	
E	6.5250×10^{1}	-4.2357×10^{2}	3.7930×10^{-1}	
F	1.0000×10^{4}	9.5872×10^{0}	-2.0539×10^{0}	1.7267×10^{6}
F	3.7274×10^{3}	-4.9818×10^{0}	-5.6633×10^{-1}	
F	9.8550×10^{1}	2.6252×10^{2}	4.8820×10^{-1}	
F	7.3250×10^{1}	3.5352×10^{2}	6.1770×10^{-1}	
G	9.5126×10^{3}	9.7756×10^{0}	-9.7222×10^{0}	-1.6826×10^{6}
G	-4.6389×10^{3}	-5.0962×10^{0}	4.3751×10^{1}	
G	4.3000×10^{2}	-3.8347×10^{2}	3.7135×10^{2}	
G	2.0000×10^{2}	1.5235×10^{2}	-5.3000×10^{-1}	
H	-2.5706×10^{4}	9.1246×10^{0}	5.1503×10^{0}	1.0470×10^{6}
H	2.0980×10^{4}	9.8864×10^{0}	-7.6177×10^{0}	
H	2.5000×10^{3}	2.2612×10^{2}	2.2422×10^{1}	
H	4.3240×10^{1}	2.2352×10^{2}	9.6364×10^{4}	

4.3 Predicted Long-Time Blade Torque Loading

After performing modal decomposition on the blade torque, inputting each mode into an LSTM for learning can obtain the characteristics of each mode over a long period. After reconstruction, the predicted long-time blade torque loading can be restored. When constructing an LSTM network model, it is necessary to select appropriate network structures, such as the number of layers, the number of neurons, etc. Historical data is used to train the LSTM network, enabling it to learn the long-term time-series characteristics of torque data. During the training process, the Mean Squared Error (MSE) is used as the loss function, and network parameters are optimized through the backpropagation algorithm. After the LSTM network is well-trained, it can output long-term torque time-series values as shown in Figure 6, which facilitates the evaluation and analysis of the stress of structural components. In this way, under limited CFD calculations, predictions equivalent to fluid-structure interaction can be achieved, and rapid rough analysis of stress distribution can be conducted to determine stress concentration areas, potential fatigue failure positions, and their patterns.

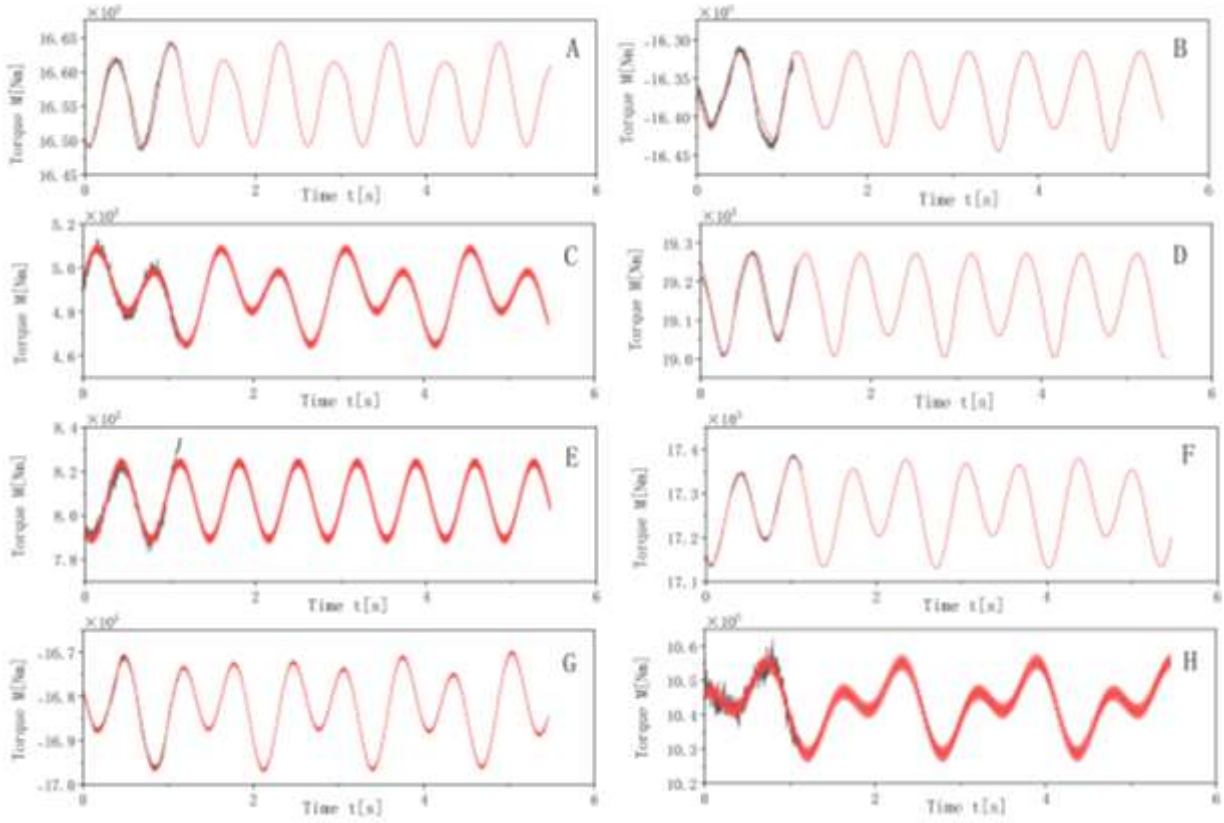

Figure 6 The predicted long-time blade torque

Figure 7 presents the torque prediction error distribution of the modal decomposition-LSTM method across eight typical operating conditions (A-H) of a hydraulic turbine. The root mean square error (RMSE) analysis reveals differential prediction performance across conditions: Conditions A, B, F and G demonstrate optimal prediction accuracy (RMSE<0.1%), confirming the method's superior capability in characterizing steady-state torque characteristics. In contrast, Conditions C, E and H exhibit relatively larger errors of 0.25%~0.5%, indicating the need for improved capture of torque pulsation features under complex flow conditions. The study demonstrates that this approach, through modal decomposition of torque loads and LSTM-based temporal prediction, achieves both high-precision reconstruction with less than 5% error in steady-state conditions and rapid stress field evaluation of critical components based on limited CFD data. This provides an effective technical solution for the digital design of turbine blades, spanning from dynamic load prediction to fatigue life assessment.

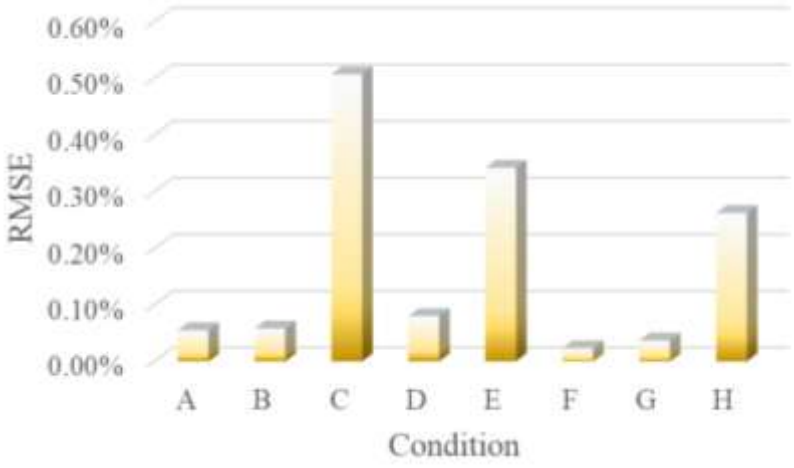

Figure 7 RMSE error of torque predictions

4.4 Fluid-Solid Interaction

4.4.1 Mesh of Structural Domain

Figure 8 is the mesh of structural domain including ear lug, connecting plane, tumbler and runner blade. The total mesh element number and node number are 375775 and 575228. The performance of materials is listed in Table 3 and are used for quasi-fluid-structure interaction (QFSI) coupling simulation by finite element method based on estimated long-time blade torque.

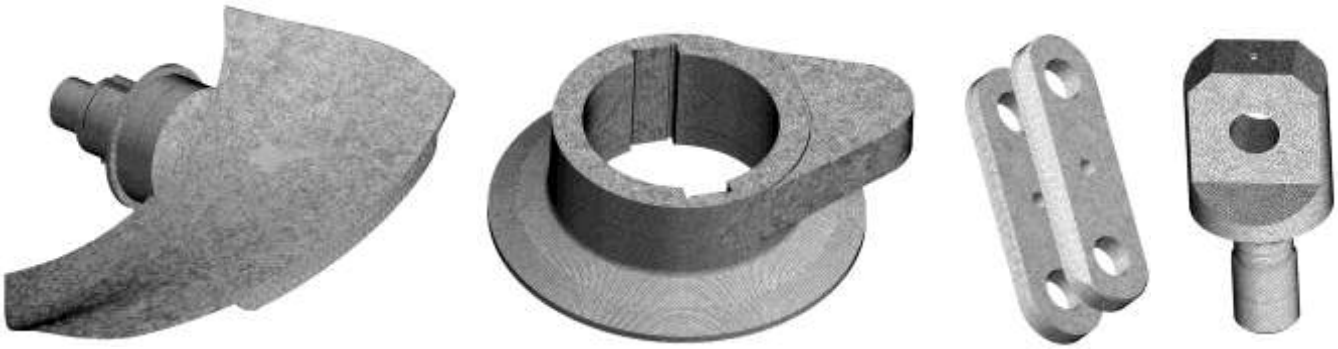

Runner Blade | Tumbler | Connecting Plate | Ear Lug

Figure 8 Mesh of structural domain for quasi-fluid-structure interaction coupling simulation

Table 3 Performance of Materials

Component	Material	Density [kg/m^3]	Young's Modulus [GPa]	Poisson's Ratio [-]	Yield Strength [MPa]	Tensile Strength [MPa]	Allowable Strength [MPa]	
							Average	Local
Runner Blade	ZG04Cr13Ni5Mo	7830	205	0.3	580	780	387	580
Tumbler	HD780CF	7850	203	0.298	670	750	447	670
Connecting Plate	ZG04Cr13Ni5Mo	7830	205	0.3	580	780	387	580
Ear Lug	34CrNi3Mo	7870	209	0.297	700	850	467	700

4.4.2 Quasi-Fluid-Structure Interaction Simulation Results

Through quasi-fluid-structure interaction simulation, the results indicate that under Conditions A-H, there are differences in the stress value distributions of the structural components. However, the locations with higher equivalent stress under different operating conditions are all concentrated in three main regions, as shown in Fig. 9. It includes the corner of the tumbler's arm, the middle of the side surface of the connecting plane, and the diameter-changing section of the thin shaft on the ear lug. Among these regions, the equivalent stress on the thin shaft of the ear lug is the highest, generally approaching the level of >500 MPa. The other regions have high stress of about 300 MPa level. Although this stress does not exceed the yield strength or tensile strength, the risk of fatigue failure is relatively high.

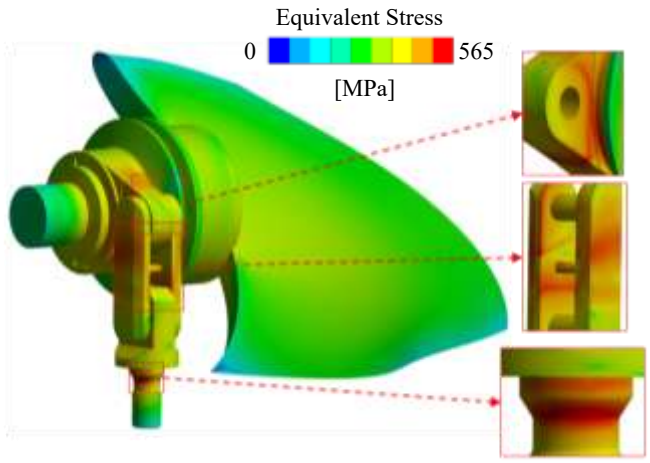

Condition A

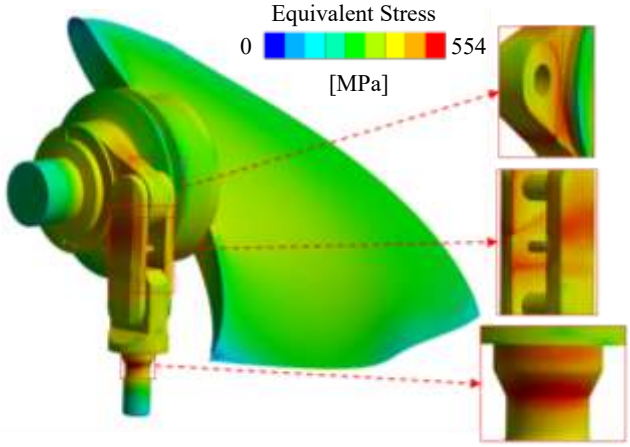

Condition B

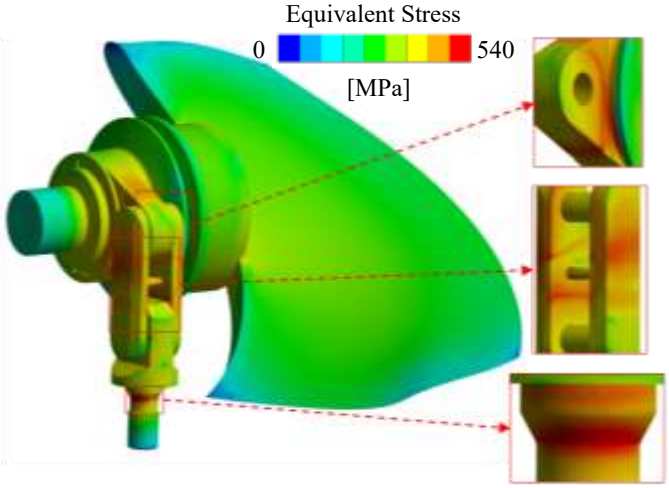

Condition C

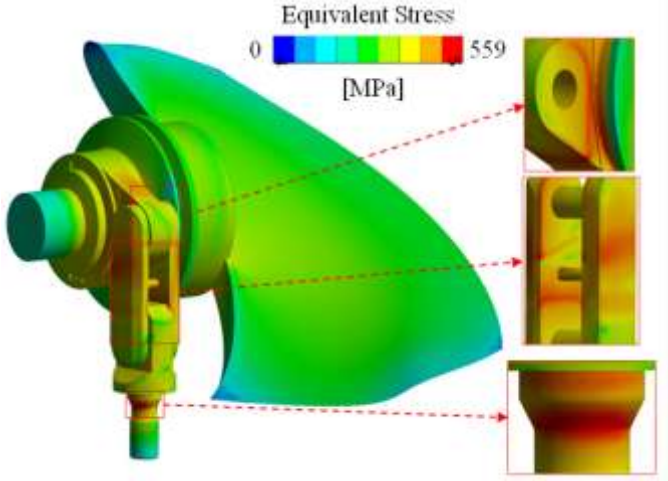

Condition D

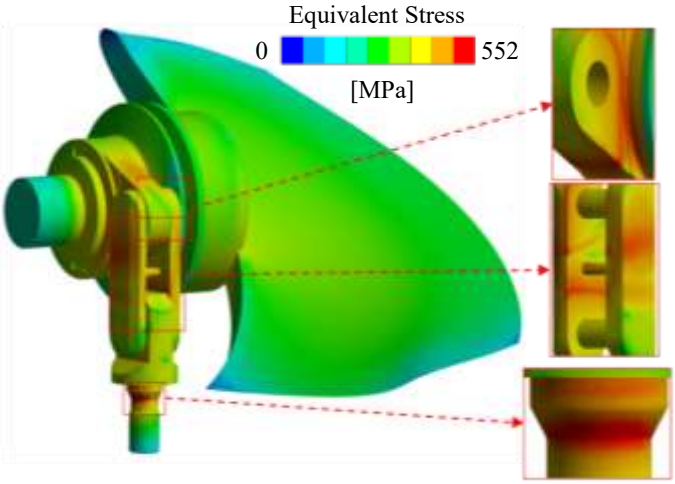

Condition E

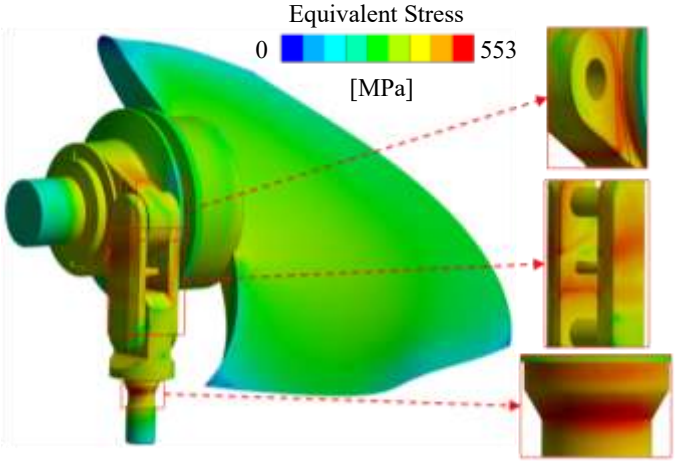

Condition F

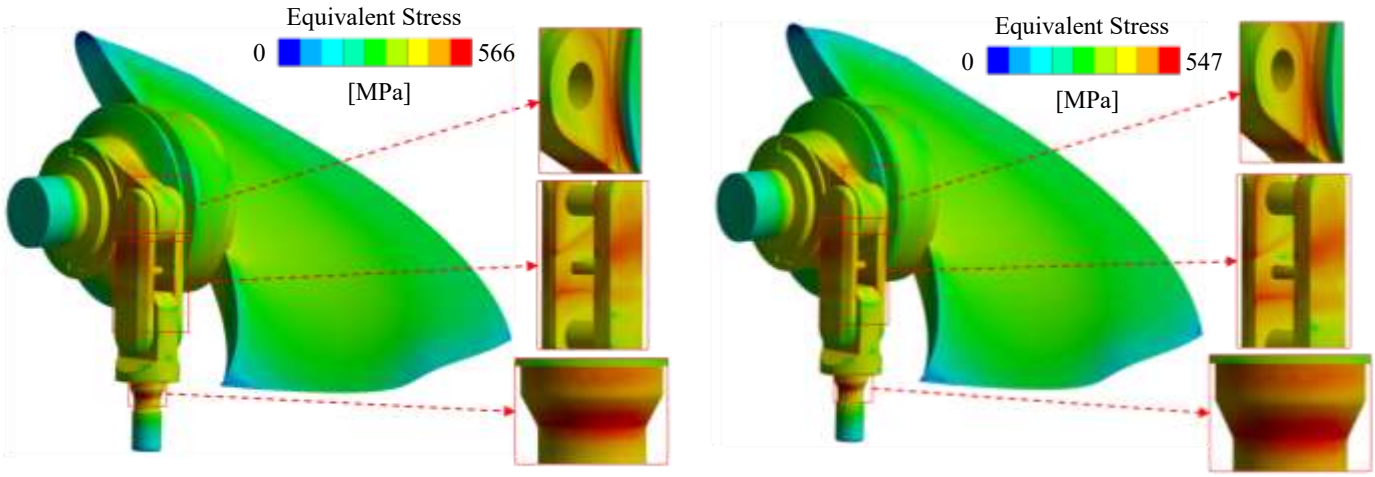

Condition G Condition H

Figure 9 Distribution of equivalent stress on blade adjustment structure

To evaluate fatigue failure, the peak-peak value of equivalent stress is important. As shown in Fig. 10, the peak-peak value of equivalent stress under different conditions are compared. Among them, condition B, E and G are higher than the other conditions. By comparing with Fig. 4, they are blade angle *b*=0 degree and -5 degrees. It means that the blade angle *b*=0 degree and -5 degrees has high amplitude of structural response of hydraulic torque variation. In Fig. 10, among the conditions, A and D are the lower two where A is *b*=-10 degrees. Positive blade angle especially a larger angle will have lower structural response amplitude.

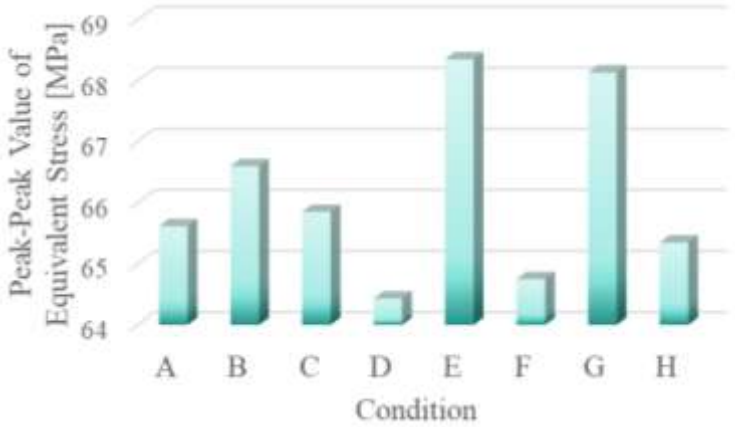

Figure 10 Peak-peak value of equivalent stress under different conditions

4.4.3 Fatigue Prediction Based on the Rainflow Counting Method

The rainflow counting method is a cyclic counting technique commonly used in fatigue analysis. Its core lies in identifying and counting stress or strain cycles within a load history, and it is primarily an algorithmic process. It begins by identifying all local extreme points (i.e., peaks and valleys) from the load history. Subsequently, the sequence of these extreme points is likened to rainflow, where each peak is envisioned as a raindrop flowing downward until it encounters a larger peak or reaches the end of the sequence. Each complete raindrop path corresponds to a full stress cycle. All complete cycles and half cycles are then counted and categorized according to their stress ranges and mean stresses.

By inputting the maximum stress change under each condition into the rainflow counting method, the mean load and amplitude load as shown in Figure 11, as well as the corresponding expected number of cycles until fatigue failure, can be obtained. This can serve as a reference for the fatigue failure characteristics of Kaplan turbines. The main load situations in condition E are relatively more complex, which also echoes Figures 4 and 10.

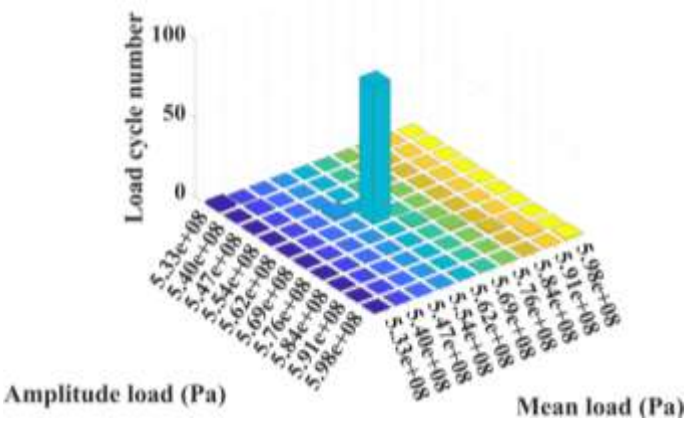

Condition A

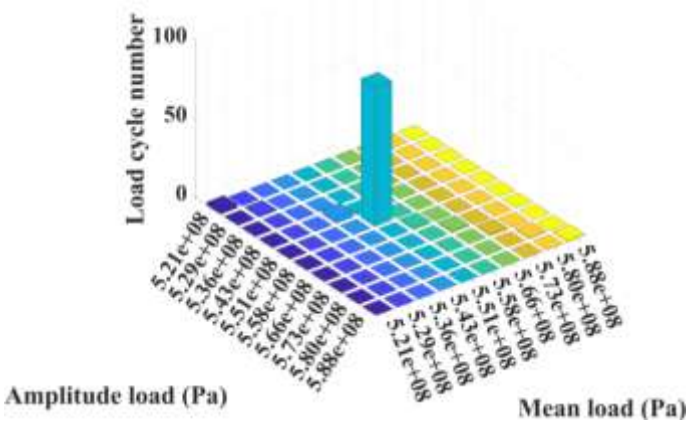

Condition B

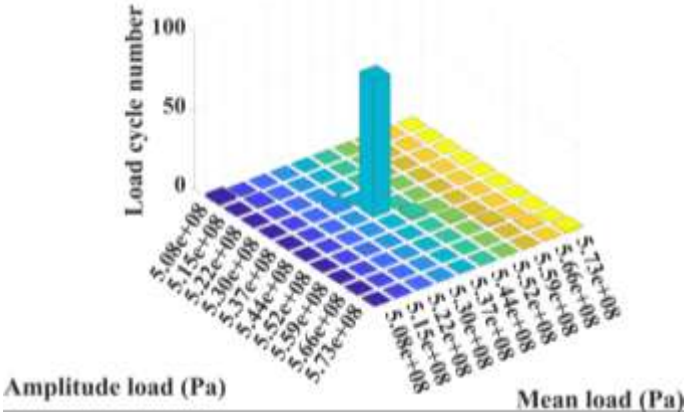

Condition C

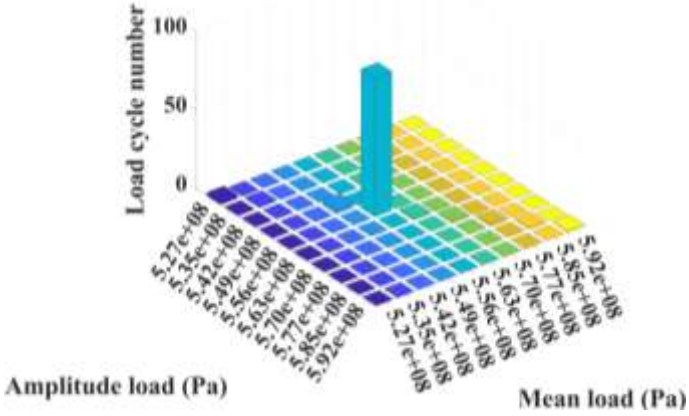

Condition D

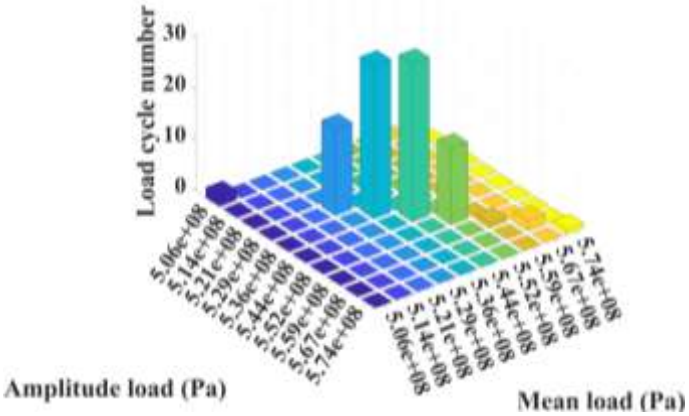

Condition E

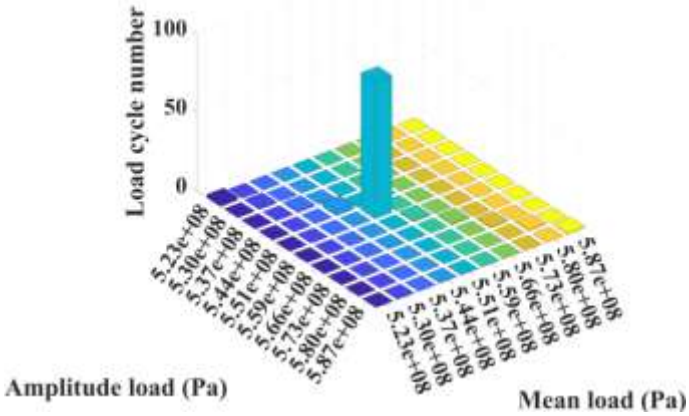

Condition F

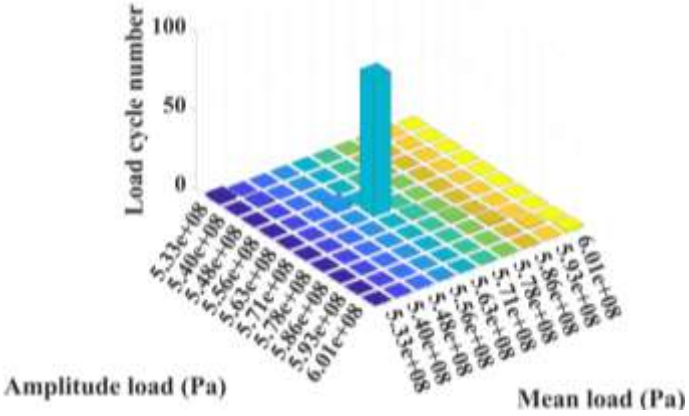

Condition G

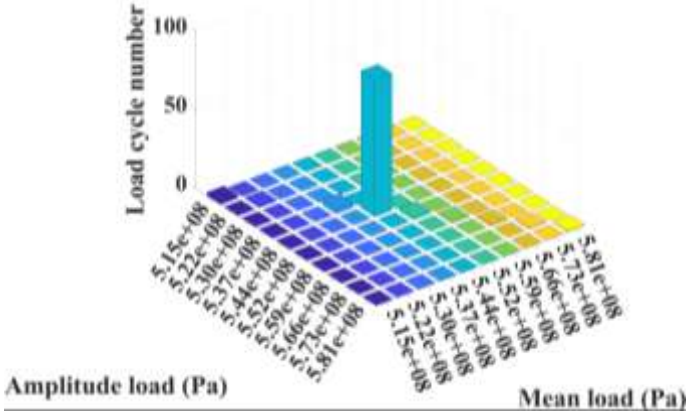

Condition H

Figure 11 Fatigue prediction based on the rainflow counting method

5 Conclusions

The conclusions can be drawn as follows:

(1) Modal decomposition of time-series signals facilitates the extraction of their primary characteristics. When combined with neural networks, it can effectively learn the underlying patterns, aiding in long-term prediction of blade torque in this case. In this study, the blade torque was processed using a combination of VMD and LSTM networks, resulting in a time-series signal that accurately describes the patterns with an RMSE ranging 0.02%~0.51% across different operating conditions, demonstrating the method's effectiveness for blade torque prediction.

(2) Under various operating conditions, there are mainly three locations on the Kaplan turbine where stresses are relatively high: the corner of the tumbler's arm, the middle of the side surface of the connecting plane, and the diameter-changing section of the thin shaft on the ear lug. Among these, the diameter-changing section of the thin shaft on the ear lug experiences the highest stress and thus requires focused attention and structural optimization to improve its strength.

(3) From the perspective of the peak-to-peak value of stress change, the runner blade angle of 0 degree and -5 degrees show the most drastic stress variation. Under the conditions of -10 degrees, the peak-to-peak value of stress change gradually decreases. The larger the runner blade angle, the safer and more stable the turbine appears. The combination of stress analysis and the full characteristic diagram can effectively illustrate the distribution of safe and stable regions.

Acknowledgements

This study is supported by the Technology Program of State Grid Fujian Electric Power Co., Ltd.; Program Title: Research on reliability technology of key components of large capacity Kaplan turbine; Grant Number: 52130424000A.

References

1. Mao X, Chen X, Yin J, et al. Research on runner characteristics of Francis turbines during power generation to no-load operation. Journal of Hydraulic Engineering, 2024, 55 (3):423-435.
2. Zhang H W, Wang L X, Liu Z Y. Research on dynamic characteristics of blade adjustment mechanism of Kaplan turbine. Journal of Hydroelectric Engineering, 2018,37(6):89-96.
3. Chen Z Q, Li M, Wu T. Fatigue Life Prediction of Turbine Runner Based on Fluid-Structure Interaction. Chinese Journal of Mechanical Engineering, 2019, 55(14): 205-213.
4. Zhao Y H, Zhou X D, Huang L. Application of Variational Mode Decomposition in Non-Stationary Signal Processing. Journal of Vibration and Shock, 2021, 40(3): 112-118.
5. Liu J G, Ma X F, Sun W. Experimental Analysis of Transient Load Characteristics in Hydraulic Turbine Governing System. Proceedings of the CSEE, 2017,37(22):6589-6596.
6. He X F, Wang Z H, Li N. LSTM-Based Fatigue Damage Prediction Model for Hydropower Units. Journal of Tsinghua University (Science and Technology), 2022, 62(5): 823-830.
7. Dong Y, Chen R Y. Optimization Design and Application Analysis of Automatic Generation Control System in Large-Scale Hydropower Plants. Lamps and Lighting, 20 23, (10): 240-242.
8. Zhang G. Analysis of Automatic Generation Control Technology for New Energy Grid Integration. Electrical Drive Automation, 2021, 43(5): 45-48.
9. Zhao S Q, Li J H. Research on the Application of Automatic Generation Control (AGC) Technology. Telecom Power Technology, 2018, 35(2): 66-67.
10. Thapa B S, Dahlhaug O G, Thapa B. Efficiency improvement of Kaplan turbine through blade profile optimization. Energy, 2015, 90: 1700-1709.
11. Davenport A G. Wind climate and building codes. Journal of the Structural Division, 19 61, 87(1): 1-22.
12. Trivedi C, Cervantes M J, Gandhi B K. Multiphysics simulation of transient loads in hydraulic turbines. Journal of Hydraulic Research, 2018, 56(3): 372-387.
13. Dragomiretskiy K, Zosso D. Variational mode

decomposition. IEEE Transactions on Signal Processing, 2014, 62(3): 531-544.
14. Zhang Q, et al. Structural response of turbine cascades under high-temperature fluid effects. Journal of Propulsion and Power, 2020, 36(4): 1234-1245.
15. Gong H, et al. Experimental study on the influence of slotted wake plates on the flow field of transonic turbine planar cascades. Journal of Aerospace Power, 2018, (12).
16. Lin JZ, et al. Experimental Technology of Pressure-Sensitive Paint in Hypersonic Wind Tunnels[J]. Acta Aeronautica et Astronautica Sinica, 2017, 38(7): 120890.
17. Li N, et al. Flow-solid coupling response of wind turbine blades under typhoon wind speeds. Journal of Wind Engineering and Industrial Aerodynamics, 2023, 234: 105234.
18. Zhang Q, et al. Analysis on wind-seismic coupling response of wind turbine tower considering blade rotation effect. Engineering Mechanics, 2021, 38(12): 1-10.
19. Gong H, Li M, Wang Q. Fluid-structure interaction analysis of large-scale wind turbines under yaw conditions. Acta Energiae Solaris Sinica, 2017, 38(5): 1234-1245.
20. Wang Q, et al. Structural dynamic response analysis of vertical axis turbines using hybrid methods. Journal of Fluids and Structures, 2016, 63: 1-15.
21. Gui Z, et al. Transient dynamic stress analysis of pump-turbine runners during startup. Journal of Hydraulic Research, 2021, 59(3): 456-467.
22. Liu Z, et al. Modal testing and analysis of turbine guide vanes. Journal of Vibration and Shock, 2020, 39(5): 123-130.
23. /Wang H T, Zhang L X, Chen M. Simulation and Experiment on Dynamic Characteristics of Blade Regulating Mechanism for Kaplan Turbine. Journal of Hydraulic Engineering, 20 21, 52(8): 945-952.
24. Xu Z P, Huang J G, Sun X F. Study on the Dynamic Instability Mechanism of Hydraulic Governing System for Hydraulic Turbines. China Mechanical Engineering, 2022,33(12): 1453-1460.
25. Li X, Zhang Q, Wang H. A hybrid VMD-LSTM framework for dynamic load prediction of hydraulic turbines. Mechanical Systems and Signal Processing, 2022,168:10 8742.
26. Hu X, et al. Prediction of runner eccentricity and Alford force of a Kaplan turbine based on variational mode decomposition. Energy Science & Engineering, 2024,12(1):1-12.